New Mexico Geological Society

Downloaded from: https://nmgs.nmt.edu/publications/guidebooks/67



Two eruptive episodes of Los Lunas Volcano: geochemistry and $^{40}Ar/^{39}Ar$ age determination using electron microprobe sample evaluation

Nelia W. Dunbar, William C. McIntosh, David W. Love, K.S. Panter, and B. Hallett
2016, pp. 203-216. https://doi.org/10.56577/FFC-67.203
Supplemental data: https://nmgs.nmt.edu/repository/index.cfml?rid=2016001

in:

Guidebook 67 - Geology of the Belen Area, Frey, Bonnie A.; Karlstrom, Karl E. ; Lucas, Spencer G.; Williams, Shannon; Zeigler, Kate; McLemore, Virginia; Ulmer-Scholle, Dana S., New Mexico Geological Society 67th Annual Fall Field Conference Guidebook, 512 p. https://doi.org/10.56577/FFC-67

This is one of many related papers that were included in the 2016 NMGS Fall Field Conference Guidebook.

Annual NMGS Fall Field Conference Guidebooks

Every fall since 1950, the New Mexico Geological Society (NMGS) has held an annual Fall Field Conference that explores some region of New Mexico (or surrounding states). Always well attended, these conferences provide a guidebook to participants. Besides detailed road logs, the guidebooks contain many well written, edited, and peer-reviewed geoscience papers. These books have set the national standard for geologic guidebooks and are an essential geologic reference for anyone working in or around New Mexico.

Free Downloads

NMGS has decided to make peer-reviewed papers from our Fall Field Conference guidebooks available for free download. This is in keeping with our mission of promoting interest, research, and cooperation regarding geology in New Mexico. However, guidebook sales represent a significant proportion of our operating budget. Therefore, only *research papers* are available for download. *Road logs*, *mini-papers*, and other selected content are available only in print for recent guidebooks.

Copyright Information

Publications of the New Mexico Geological Society, printed and electronic, are protected by the copyright laws of the United States. No material from the NMGS website, or printed and electronic publications, may be reprinted or redistributed without NMGS permission. Contact us for permission to reprint portions of any of our publications.

One printed copy of any materials from the NMGS website or our print and electronic publications may be made for individual use without our permission. Teachers and students may make unlimited copies for educational use. Any other use of these materials requires explicit permission.

This page is intentionally left blank to maintain order of facing pages.

New Mexico Geological Society Guidebook, 67th Field Conference, Geology of the Belen Area, 2016, p. 203-216.

TWO ERUPTIVE EPISODES OF LOS LUNAS VOLCANO: GEOCHEMISTRY AND $^{40}AR/^{39}AR$ AGE DETERMINATION USING ELECTRON MICROPROBE SAMPLE EVALUATION

Nelia W. Dunbar[1], William C. Mcintosh[1], David W. Love[1], K.S. Panter[2], and B. Hallett[3]

[1]New Mexico Bureau of Geology and Mineral Resources, 801 Leroy Pl., Socorro, NM 87801;
[2]Bowling Green State University, Bowling Green, OH 43403;
[3]Matanzas Geoscience, 77 Saragossa St., St. Augustine, FL 32084

Abstract—A study of 86 samples of trachyandesitic and dacitic lava and cinders from the Los Lunas volcano, central New Mexico, demonstrates the volcano consists of two overlapping but temporally and compositionally distinct eruptive edifices differing in age by 2.56 Ma. Lava compositions at Los Lunas volcano are consistent with other lavas found in the Rio Grande rift, but, based on major and trace element determinations, no simple model can be proposed to genetically link the two dominant magma compositions. Rather, the two magma batches appear to have been independently generated, consistent with the large age gap between eruptions of the two edifices. An experiment carried out as part of this study indicates that the accuracy and precision of $^{40}Ar/^{39}Ar$ dates for young mafic to intermediate lavas can be maximized by selecting samples that contain K-feldspar as a late-crystallized phase, and contain little or no glass or alteration phases. Characterization of samples was undertaken using the electron microprobe, where samples were ranked on a scale of 1 to 10 (with 10 being most suitable for dating) based largely on whether the K in the sample could be determined to be housed in extremely fine-grained feldspar interstitial to more abundant phenocryst phases, or was in residual volcanic glass. Sample rating was downgraded if the sample showed evidence of chemical alteration. The $^{40}Ar/^{39}Ar$ results from the most highly rated samples yield an age of 3.83±0.05 Ma for the Southwest Edifice of Los Lunas volcano. This volcanic center is physically overlapped by the 1.271±0.014 Ma Main Edifice. The absolute ages agree with relative ages determined from geological mapping. Within the Main Edifice, field relationships indicate a sequence of five eruptive events. The ages of the best samples from the Main Edifice all agree within analytical error, suggesting that the entire period of eruptive activity spanned less than 100,000 years. The precision and accuracy of data in this study were much enhanced by using microprobe observations of groundmass glass and K-feldspar to aid in the sample selection process. Sample selection based only on thin section observations would have yielded lower quality data, because the degree of crystallization of residual glass would have been incompletely assessed.

INTRODUCTION

Determining accurate ages of basaltic to intermediate volcanic rocks using the $^{40}Ar/^{39}Ar$ method can be difficult due to the presence of atmospheric, excess, or inherited argon, which may be large compared to the radiogenic ^{40}Ar, especially in young, low-potassium (K) samples (Dalrymple and Moore, 1968; Dalrymple, 1969; Koppers et al., 2000). In some cases, excess or inherited ^{40}Ar may reside in xenocrysts, phenocrysts or melt inclusions within phenocrysts (Esser et al., 1997; Winick et al., 2001). Many samples of phenocryst-free, finely crystalline to glassy groundmass have also yielded $^{40}Ar/^{39}Ar$ or K-Ar age determinations that are inaccurate and/or imprecise (Singer and Pringle, 1996; Singer et al., 1998 Koppers et al., 2000). In particular, samples with optically identifiable groundmass glass are prone to yielding low-precision results with low radiogenic yields (percentage of non-atmospheric ^{40}Ar) and anomalously young or old apparent ages (Fleck et al., 1977; Foland et al., 1993). In the field, many workers prefer to sample flow interiors that appear holocrystalline, but these are not always available or exposed, especially in very young, non-eroded lavas.

The electron microprobe offers a means of assessing and quantitatively analyzing basaltic to intermediate groundmass features that are too small to be assessed optically. X-ray mapping and quantitative analyses allow accurate characterization of crystal and glass phases as small as 2 μm. The crystallinity of small interstices, difficult to evaluate using a petrographic microscope, can be quantitatively assessed by multiple analyses of interstitial material, where homogeneous compositions indicate glass, and heterogeneous compositions indicate multiple crystal phases. Towards the goal of effectively using the electron microprobe to assess the quality of low-K lava samples for $^{40}Ar/^{39}Ar$ dating, we have devised procedures for evaluating the dating potential of mafic to intermediate lava samples. These procedures consist of systematically assessing the abundance of glass, presence or absence of potassic feldspar, and presence of alteration phases in a given sample using backscattered electron imaging, elemental mapping, and quantitative analysis. Each sample is then rated on a 1-to-10 scale (10 being best) based on combined observations. Subsequent dating of rated samples then allows sample rating and age quality to be compared.

We chose the Los Lunas volcano, located just south of Albuquerque, in central New Mexico, as a test area for this study. During a mapping project conducted under the U.S. Geological Survey's National Cooperative Geologic Mapping Program, a suite of 86 samples was collected from the volca-

no, targeting both the older-appearing Southwest Edifice, and the younger-appearing Main Edifice. Where possible, samples were collected from stratigraphic sections consisting of multiple lavas. A wide range of sample types was collected, from highly crystalline samples of lava interiors to samples of much glassier flow tops and bottoms.

Petrography and whole rock geochemical analyses were carried out on a subset of samples to examine the evolution of the volcanic edifices. A second subset of samples was then examined using an electron microprobe and rated for suitability for $^{40}Ar/^{39}Ar$ dating. We assessed mineralogy and crystallinity, with particular focus on examining the fine-grained groundmass found between phenocrysts, which may be composed of glass, of very fine microlites, or a combination of both. The ages of selected higher quality samples were then determined by $^{40}Ar/^{39}Ar$ analysis. Our hypothesis was that samples containing more glass, even among the higher quality samples, would yield ages that are less accurate and precise.

BACKGROUND

Los Lunas Volcano

Los Lunas volcano, located west of the town of Los Lunas, and characterized by two large, intersecting white "Ls" decorating the northeast-facing flank, rises dramatically above the terraces of the Rio Grande Valley. The volcano is composed of a series of lava flows and pyroclastic materials, with compositions that are more evolved than basalt (Kelley and Kudo, 1978). The Los Lunas volcano appears to consist of two distinct eruptive centers (Fig. 1). The largest, more northerly part of the volcano (here called the "Main Edifice") includes two prominent lava lobes that extend to the E and SE from the summit. The Main Edifice consists of at least five eruptive units (four lavas and one pyroclastic deposit) and has been faulted and uplifted 150 m above the surrounding topographic top of basin fill (Love et al., 1998; Panter et al., 1999). Lavas in the Main Edifice are well exposed and reveal a wide range of textures. Published K-Ar dates of some Main Edifice lavas range from 1.1 to 1.3 Ma (Bachman and Mehnert, 1978).

Southwest of the Main Edifice of Los Lunas volcano, lavas and pyroclastic rocks are exposed inset of low, hummocky hills referred to here as the "Southwest Edifice." The Southwest Edifice is darker in color than the Main Edifice, which has a brownish appearance. The Southwest Edifice has a jumbled appearance, probably due in part to slumping, and consists of a series of four volcanic units, including lavas and pyroclastic materials (Panter et al., 1999). These authors also reported several intrusive bodies thought to be related to the southwestern eruptive center. Kelley and Kudo (1978) note textural differences between the more crystal-rich "southwestern andesites" (our "Southwest Edifice") and the more aphanitic, fluidal appearing lavas of the Main Edifice. Previously reported chemical compositions of samples of the Southwest Edifice are more evolved than those of Main Edifice lavas (Kasten, 1977).

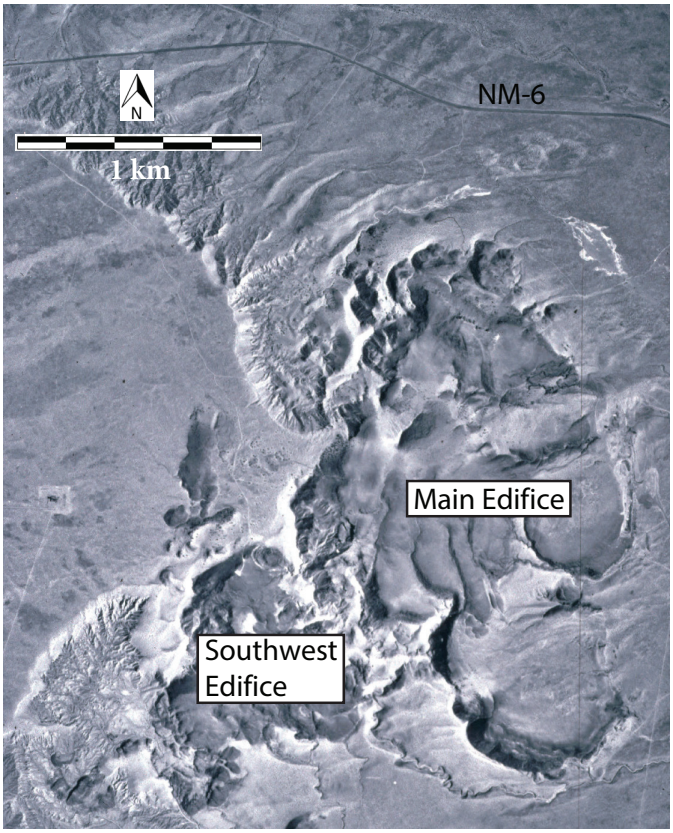


FIGURE 1. Aerial photograph of Los Lunas volcano, showing the Main Edifice and the Southwest Edifice. Location of NM Highway 6 is shown for reference.

METHODS AND RESULTS

Sampling

During geologic mapping of Los Lunas Volcano, a suite of 86 volcanic samples was collected of lavas and pyroclastic materials (see Supplementary Documentation Table 1). A range of sample types was collected based on field observations, ranging from glassy to highly crystalline. Subsets of these samples were used for the analyses described below. As described in Supplementary Documentation Table 1, the sample numbering in this project did not remain consistent through the life of the project. Different prefixes were used for samples collected at different times (98LL vs LLV), and the same samples analyzed in different laboratories were not always given the same prefix. However, for all samples, the numeric part is a unique identifier. In the body of the paper, we refer to the samples only by the numeric identifier. However, in some of the figure and tables, and in supplementary documentation, the lab-specific identifier is used.

Petrography

A total of 41 representative lava samples were examined for texture and mineralogy using standard petrographic techniques. The samples observed in thin section range from porphyritic to microporphyritic (1-15 vol.%), are variability

vesicular, and their groundmass textures vary from holocrystalline to hypocrystalline (crystals plus glass). The majority of the samples contain phenocrysts of plagioclase, two pyroxenes and accessory opaque oxides. However, there are notable differences in texture and mineralogy between Main Edifice and Southwest Edifice lavas. Southwest Edifice lavas tend to contain more glass, more commonly display trachytic textures (i.e. aligned plagioclase) and have higher phenocryst contents (5-15 vol.%) relative to Main Edifice lavas, although their mineral assemblage is less diverse. In addition to the plagioclase and pyroxenes that predominate in Southwest Edifice lavas, many of the Main Edifice lavas also contain amphibole and biotite as well as minor olivine and accessory apatite.

Whole Rock Geochemistry

A total of 46 samples were analyzed for major, minor and trace elements (V, Cr, Ni, Cu, Zn, Ga, Rb, Sr, Y, Zr, Nb, Ba and Pb) by X-ray fluorescence (XRF) on a Philips PW2400 XRF spectrometer at the New Mexico Bureau of Geology and Mineral Resources. The samples were prepared as fused glass beads (for major element determinations) and pressed powder samples (for trace elements). To measure loss on ignition (LOI), the samples were first dried at 110°C for 2 hours (to removed adsorbed H_2O), and then heated to 1000°C for 2 hours for the actual LOI measurement. XRF analyses used an end-window Rh tube to produce X-rays, and a P-10 gas low detector, Xe counter and scintillation detector. Analytical precisions for major elements with concentrations >1 wt % are <0.1% (1σ) and for trace elements are typically <4% (1σ). Precision can be evaluated by examining replicate analyses (supplementary documentation Table 1). Major- and minor- element data used in plots are recalculated on a 100% volatile-free basis with total Fe as FeO. Representative analyses are provided in Table 1 (see supplementary documentation Table 1 for all analyses). The whole-rock samples fall into two groups of intermediate composition; those from the Main Edifice that cluster in the trachyandesite field and those from the Southwest Edifice that cluster about the intersection of four compositional fields and are hereafter referred to as dacite (Fig. 2). Outliers of these groups consist of a slightly more mafic basaltic trachyandesite (sample 57) from the Main Edifice and a slightly alkali-depleted andesite tephra (sample 18) from the Southwest Edifice (Fig. 1, Table 1). Additionally, two electron microprobe analyses of interstitial glass from lavas of the Main Edifice fall within the trachydacite and rhyolite fields.

Fundamentally, the compositions of the Main Edifice are distinguished from the Southwest Edifice by total alkali concentration and silica saturation. The trachyandesites of the Southwest Edifice lie on the alkaline and subalkaline boundary (Fig. 2) whereas the dacite of the Main Edifice is exclusively subalkaline. Both trachyandesite and dacite are oversaturated with respect to silica, although the dacites have higher *Q*-normative contents (12 to 18 wt.%) relative to the trachyandesite (0.5 to 8 wt.%). The dacites have higher concentrations of SiO_2 (>60 wt.%) relative to trachyandesites (≤60 wt.%), but their average Mg-numbers are similar (~48; Table 1).

In general, lava compositions at Los Lunas are comparable to other intermediate rocks within the Rio Grande rift, including pre-caldera rocks from the Jemez Mountains volcanic field (JMVF; Figs. 3 and 4). Los Lunas samples show a systematic decrease in TiO_2, FeO_t and P_2O_5 with increasing SiO_2 concentration between trachyandesite and dacite (Fig. 3A-C). However, a more complex relationship between magma types from the two edifices is indicated by data trends for MgO, K_2O and CaO when plotted against SiO_2 (Fig. 3D-F). The trace elements Sr, Ba and Zr also decrease with increasing SiO_2 (Fig.4A-C). However, Rb displays a comparable range in concentrations for both trachyandesite and dacite (Fig. 4D). Chromium content increases with increasing silica content, which is likely caused by the higher volume percentage of clinopyroxene (± spinel) phenocrysts within Southwest Edifice lava relative to Main Edifice lava. The Ba concentrations in Main Edifice trachyandesites are significantly elevated relative to intermediate compositions from the Jemez Mountains volcanic field (Fig. 4B).

Electron Microprobe Analysis

Polished microprobe mounts of 86 Los Lunas volcano samples were examined using a Cameca SX-100 electron microprobe housed at the New Mexico Bureau of Geology and Mineral Resources. The samples were mounted in epoxy resin, and polished using deionized water and pure diamond powder, with the final polishing step using 2-µm grit.

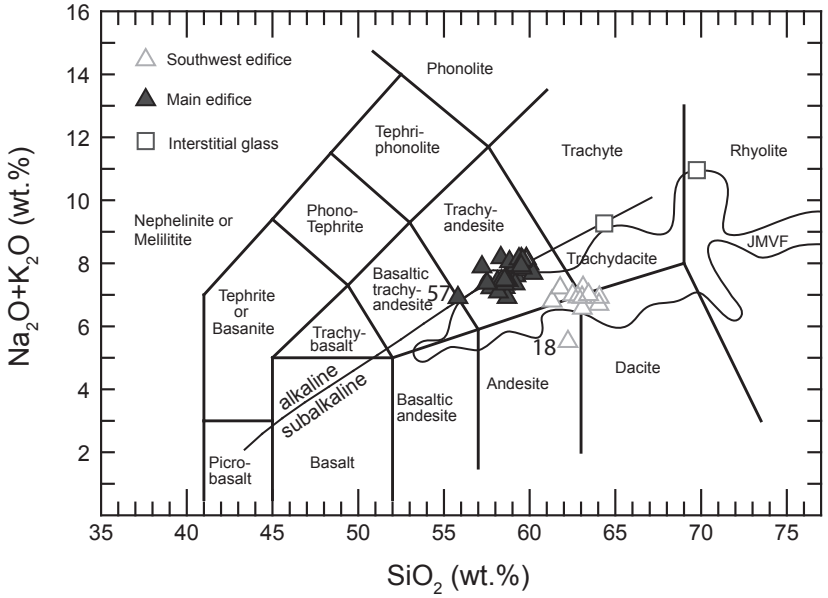


FIGURE 2. Total alkali-silica diagram for whole rock samples from Los Lunas volcano. Line separating alkaline and subalkaline rocks after Irvine and Braragar (1971) The composition field of rocks from the Jemez Mountains volcanic field (JMVF) is from Rowe et al. (2007).

TABLE 1: Geochemistry of representative Los Lunas volcanics.

sample	**LLV08**	**LLV11**	**LLV13**	**LLV16**	**LLV22**	**LLV29**	**LLV31**	**LLV39**	**LLV41**	**LLV42**
edifice*	SW	SW	SW	SW	CE	CE	CE	CE	CE	CE
*rock type***	*dacite*	*TA*	*dacite*	*dacite*	*TA*	*TA*	*TA*	*TA*	*TA*	*TA*
SiO2	62.54	60.25	61.57	61.56	58.73	56.66	56.79	57.23	57.65	57.91
TiO2	0.68	0.84	0.72	0.72	0.91	0.99	1.01	1.03	0.99	0.98
Al2O3	15.70	15.94	16.29	15.92	16.26	16.06	16.44	16.33	16.42	16.40
Fe2O3	4.86	5.46	5.11	5.13	5.92	6.60	6.70	6.90	6.51	6.40
MnO	0.08	0.09	0.09	0.08	0.10	0.11	0.11	0.11	0.10	0.10
MgO	2.36	2.68	2.40	2.56	2.66	3.41	3.46	3.57	3.35	3.21
CaO	4.78	5.20	5.18	4.99	5.55	5.92	6.63	6.17	6.06	6.06
K2O	3.20	2.96	2.46	2.59	2.94	2.45	2.40	2.34	2.43	2.51
Na2O	3.55	4.07	3.95	4.16	4.89	4.22	4.70	4.63	4.79	4.82
P2O5	0.35	0.57	0.35	0.42	0.72	0.79	0.80	0.75	0.80	0.80
LOI	1.64	1.89	1.30	1.14	1.18	2.36	0.47	0.57	0.07	0.19
total	99.74	99.95	99.42	99.27	99.86	99.57	99.51	99.63	99.17	99.38
Mg #	49	49	48	50	47	51	51	51	50	50
V	58	73	70	69	76	115	83	106	108	99
Cr	44	38	35	46	24	29	22	27	28	30
Ni	26	29	21	28	22	27	21	25	29	30
Cu	23	25	21	25	18	31	28	27	39	40
Zn	66	76	68	71	82	87	77	76	79	79
Ga	19	19	19	19	20	20	20	20	21	21
Rb	36	39	29	33	39	37	46	37	35	34
Sr	739	1025	869	922	1414	1701	1384	1634	1600	1601
Y	23	23	20	22	24	22	24	21	22	22
Zr	234	240	192	217	278	229	280	234	227	226
Nb	22	34	19	25	64	69	65	70	68	68
Ba	1827	1566	1370	1686	2218	2250	2139	2338	2376	2380
Pb	14	14	14	14	13	20	17	16	16	16
Th	5	10	6	8	20	23	18	20	18	20
U	2	2	1	2	4	4	3	4	4	4

Major elements are given in wt.%, trace elements in ppm, both measured by XRF. LOI = loss on ignition
Mg #, atomic % Mg/(Mg+Fe^{2+}), where Fe^{2+} is calculated using FeO = 0.9(Fe_2O_3). TA = trachyandesite
* SW is the Southwestern Edifice, ME is the Main Edifice
** TA is trachyandesite

One of the objectives of this investigation was to determine the sample crystallinity, particularly on a finer scale than could be discerned using a conventional petrographic microscope. This was done using backscattered electron (BSE) imaging, in which phases with higher mean atomic number appear brighter than those with lower atomic number. The resolution of the technique is around 1 µm. BSE was used to assess the degree of crystallinity, particularly of the material interstitial to phenocrysts or microlites. A second objective was to determine the location of the K in the sample, particularly whether the K was present in glass or had been incorporated into potassium-bearing feldspar. Potassium is the radioactive element that produces the ^{40}Ar used in the $^{40}Ar/^{39}Ar$ dating technique, so determining the location of K and the type of K-bearing phases (feldspar or glass) can help predict the quality of an $^{40}Ar/^{39}Ar$ date.

Also, one of the primary objectives of the study was to examine the quality of the $^{40}Ar/^{39}Ar$ geochronology results of samples as a function of the phase in which K is dominantly located. Initial examination included simple backscattered electron imaging, followed by collection of 2-dimensional maps of the K distribution across the sample surface and quantitative analysis of mineral phases and glass. The K maps were col-

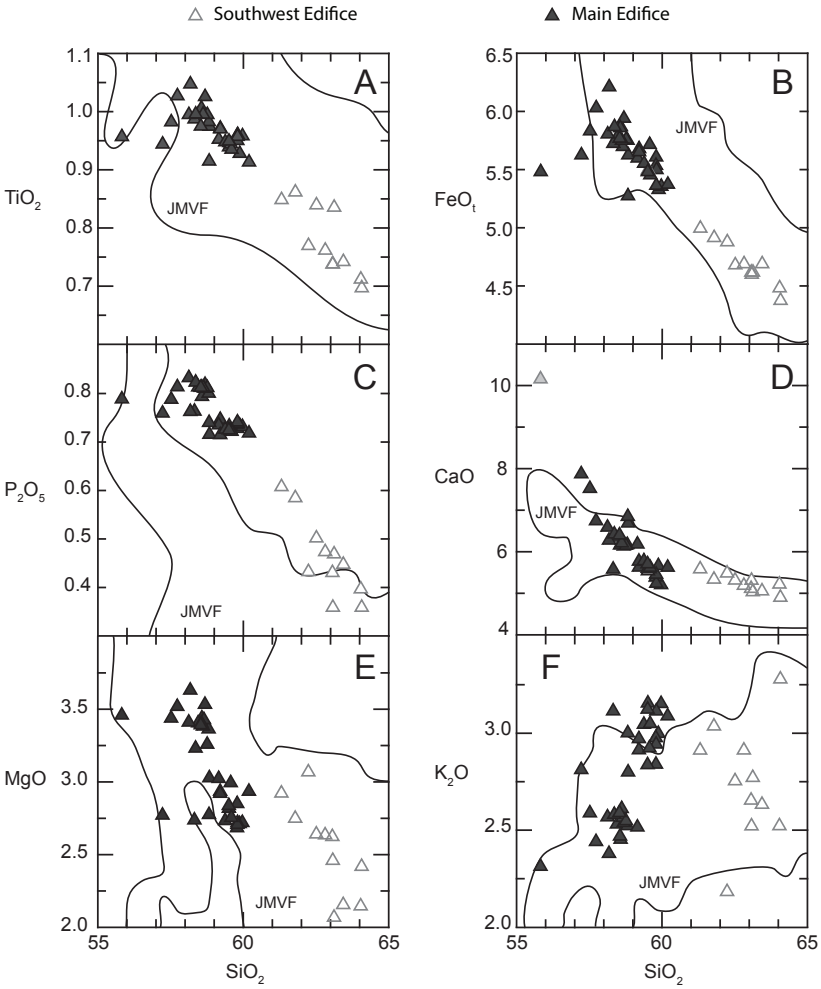


FIGURE 3. Variation of selected major elements with silica content (all in weight % oxides). Fields delimiting Jemez Mountains volcanic field (JMVF) rocks from Rowe et al. (2007).

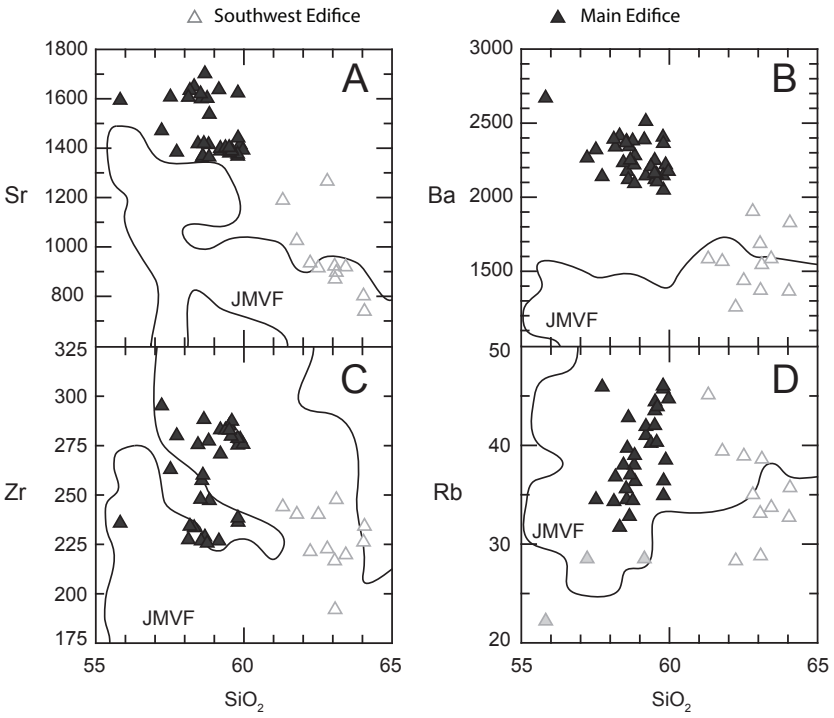


FIGURE 4. Variation of selected trace elements (in ppm) with SiO_2 (wt.%). Jemez Mountains volcanic field (JMVF) rocks from Rowe et al. (2007).

lected at a 512x512-pixel resolution, with a total collection time of around 45 minutes. An accelerating voltage of 15 kV was used, and a probe current of 20 nA, with a 1 micrometer focused beam. The K maps provide insight into whether the K was uniformly distributed in a glassy phase, or whether it was concentrated in small (as small as 2 μm) K-bearing feldspar crystals in interstices between larger crystalline phases, or as potassic rims on plagioclase.

Some otherwise well-crystallized samples were found to contain small amounts of groundmass glass in interstices between crystals; in these cases, virtually all K was concentrated within the glass. In other samples the groundmass was fully crystallized, and K resided in K-feldspar, either as thin (<10 μm) rims on plagioclase or as fine (<15 μm) groundmass crystals intergrown with albite. This K-feldspar would be impossible to identify optically due to the small grain size and intergrown nature of the crystals.

Different samples from Los Lunas volcano exhibit different degrees of crystallinity, when examined in BSE (Fig. 5). Image A (sample 86) is from a sample that contains abundant glass and few crystals. Two plagioclase laths are labeled on the image, and a number of small, bright Fe oxide grains can be seen, but the overall uniform gray shade of the imaged material indicates chemical homogeneity, which, in this case, represents volcanic glass. Image B shows the K distribution across an inset area of image A. The K distribution is very uniform, except for areas of vesicles or plagioclase. Image C (sample 74) represents a sample that contains significantly more plagioclase laths and Fe oxide microlites, but the K distribution (image D) is uniform within the groundmass of the sample, again suggesting that the groundmass is chemically homogeneous, and represents volcanic glass. Images E and F (sample 41), in contrast, represent a sample in which the groundmass appears to have fully crystallized. When observed at high magnification, the areas between the larger crystals appear mottled in backscattered electron imaging, as well as with respect to K distribution. The K map (image F) shows a patchy appearance, that we interpret to represent fine-grained, intergrown, alkali feldspar in the groundmass between plagioclase laths. The rims of some of the plagioclase laths also appear to be more K-rich than the cores.

In order to help interpret the images described above, a second component of microprobe analysis focused on quantitative analysis. Phases analyzed included feldspar, pyroxene, amphibole, olivine, and interstitial glass. Representative analyses are presented in Table 2, and the complete body of analytical data is available in Supplementary Documentation Table 2. Elements analyzed varied for different minerals, and are presented as footnotes to Table 2, along with count times, and analytical precision based on replicate analysis of standards. For all minerals, an accelerating voltage of 15 kV and probe current of 20 nA were used. Pyroxene, amphibole and olivine were analyzed with a 1-μm beam size, and for feldspar, a beam diameter of 10 μm was used to avoid Na loss. For glass, an accelerating voltage of 15 kV was used, and a probe current of 10 nA. Although typical glass analyses are done with a defocused electron beam (up to 25 μm), the groundmass of samples examined here was typically analyzed with a 10-μm beam because of the small size of available microlite-free glass or groundmass areas (see Fig. 5). Some points had to be analyzed with a 5-μm beam diameter, which may have led to sodium volatilization (Nielsen and Sigurdsson, 1981). Care was taken, using backscattered electron imaging, to select the most microlite-free glassy areas for analysis. Beam sizes for individual analyses of most glass or groundmass points are given in Supplementary Documentation Table 2. A number of standard reference materials, including feldspars, amphiboles, and glasses, were run as unknowns in each analytical session to monitor calibration accuracy, and inter-run reproducibility (see Supplementary Documentation Table 2).

The mafic silicates pyroxene, amphibole, and rare olivine were analyzed as part of general sample characterization, but the geochemistry of those phases is not examined in this study. Nevertheless, representative analyses are presented in Table 2, and full datasets are available in Supplementary Documentation Table 2. Two pyroxenes, augite and clinoenstatite, are present in many samples. Amphibole was recognized in a number of samples. Rare olivine was observed, and where analyzed, was determined to be Mg-rich. Other phases, including biotite and apatite, were observed petrographically but were not analyzed.

Of particular interest in this study, because of the emphasis on understanding which samples are best suited for $^{40}Ar/^{39}Ar$ dating, was geochemical analysis of the feldspar, and the groundmass material between the plagioclase laths. The plagioclase composition ranges between bytownite and andesine, with most compositions in the andesine-labradorite range (An_{32}-An_{55})**.** The smaller feldspar microlites are more sodic and potassic than the cores of large plagioclase (Fig. 6). A plot of SiO_2 and K_2O shows a positive correlation between these two elements, and also shows that the feldspar rims are generally more potassic than the feldspar cores (Fig. 7). Coupled with analysis of feldspar, analyses were also carried out in the interstitial areas between feldspar laths. In the examples presented here, the interstitial material in samples LLV86 and LLV74 is chemically consistent with being volcanic glass (Table 2). The Si-to-Al ratio in these analyses is lower than is typical for feldspar, the Fe is more elevated than would be expected in feldspar, and the material contains significant Cl, which is not compatible in the structure of feldspar, but is found in volcanic glass. The chemical composition of the interstitial glass is more evolved than the whole rock composition (Fig. 2), and is more evolved for the more crystalline sample (74) than for the sample that contains few crystals (86). In contrast, the composition of interstitial material in the most crystalline sample (41) is chemically consistent with being feldspar (Table 2). The higher Al_2O_3 content, lower FeO content, lack of MgO and TiO_2, and absence of Cl all support this interpretation. When plotted on a feldspar ternary diagram (Fig. 6), the composition of most of the interstitial material plots in the anorthoclase field. However, the "patchiness" of the interstitial areas, when observed in BSE and in the maps of K distribution, suggest that the interstitial areas contain multiple phases, probably including potassic and sodic feldspars that are closely intergrown.

Samples were rated on the basis of glass content versus K-feldspar content, and given ratings from 1 to 10. A completely holocrystalline sample, in which all of the K would be contained in feldspar, would be rated 10, and a sample with completely glassy groundmass would be rated 1. Samples in between these two end members would be rated, somewhat subjectively, based on the ratio of finely crystalline vs. glassy interstitial material. If a sample showed evidence of alteration, particular breakdown of olivine and associated presence of iddingsite or clay minerals, the numeric ranking, based on crystallinity, would be downgraded. Based on the ratings, a group of 19 higher rated samples (ratings from 6 to 10) were selected as suitable for $^{40}Ar/^{39}Ar$ dating. Detailed descriptions of individual samples, and resultant ranking can be accessed in Supplementary Documentation, Table 2.

Argon Geochronology

Groundmass concentrates were prepared from the 19 selected samples by crushing, sieving, washing in dilute HCl, Franz magnetic separation, and hand picking to remove remaining phenocrysts. Samples and Fish Canyon Tuff sanidine monitors (28.201 Ma; Kuiper et al. (2008)) were packaged in machined aluminum discs and irradiated at the Texas A & M reactor for 80 minutes. Monitor and unknowns were analyzed at the New Mexico Geochronological Research Laboratory. Single crystals of monitor sanidine were fused by CO_2 laser fusion, and groundmass concentrates were incrementally heated in a resistance furnace. Isotopic measurements were performed using an MAP 215-50 mass spectrometer. Results are detailed in Figures 8 and 9, with more details supplied in Supplementary Documentation Table 3, and are summarized in Figures 10 and 11 and Table 3. Additional details regarding analytical parameters are provided in the footnote to Table 3 and Supplementary Documentation Table 3.

Age spectra from the 19 analyzed samples are variably discordant at low- and high-temperature steps, but all have central flatter intervals that yield plateau ages (Figs. 8 and 9); plateau criteria: three or more contiguous steps, constituting > 50% of ^{39}Ar released, that agree in age within two sigma uncertainty (Fleck et al., 1977). Figure 10 shows all plateau ages, demonstrating that the plateau ages are strongly bimodal, with Main Edifice plateau ages ranging from 1.07±0.11 Ma

TABLE 2. Representative Compositions of minerals and glass from the Main Edifice (ME) and Southwest Edifice (SWE) components of Los Lunas Volcano as analyzed by electron microprobe.

Sample #	Location	Notes	P_2O_5	SiO_2	SO_2	TiO_2	Al_2O_3	MgO	CaO	MnO	FeO	SrO	BaO	Na_2O	K_2O	F	Cl	Total	beam size
			wt.%	wt.%	wt.%	wt.%	wt.%	wt.%	wt.%	wt.%	wt.%	wt.%	wt.%	wt.%	wt.%	wt.%	wt.%		(microns)
Pyroxene*																			
LLV8-1	SWE	large core		53.88		0.20	1.99	27.88	1.34	0.30	14.09			0.04	0.02			100.19	
LLV8-4	SWE	small core		54.33		0.19	1.47	27.73	1.29	0.34	14.69			0.04	0.00			100.37	
LLV9-2	SWE	large core		50.98		0.54	2.99	15.83	20.22	0.24	8.29			0.41	0.00			99.83	
LLV9-3	SWE	small core		50.36		0.72	3.43	15.46	20.68	0.25	8.60			0.37	0.03			100.03	
LLV64-10	ME	small core		54.32		0.54	1.38	28.63	1.94	0.56	13.03			0.05	0.02			100.52	
LLV64-11	ME	large core		56.24		0.52	2.07	27.65	1.40	0.68	11.05			0.19	0.34			100.13	
LLV-20-9	ME	small core		50.43		1.04	3.01	15.75	19.87	0.35	7.77			0.71	0.09			99.02	
LLV64-8	ME	small core		51.75		0.54	3.12	15.89	19.82	0.21	7.98			0.69	0.02			100.11	
Amphibole*																			
LLV-22-6	ME	large core		41.65		3.06	11.40	13.20	10.58	0.18	13.20			2.57	0.84			96.73	
LLV-22-7	ME	large rim		41.14		3.62	12.04	13.72	10.72	0.16	12.00			2.67	0.92			97.03	
Olivine*																			
LLV-29-5	ME	large core		39.01		0.05	0.00	43.71	0.14	0.49	16.93			0.00	0.00			100.33	
Feldspar**																			
LLV8-6	SWE	large core		54.51			27.73		10.49		0.78			5.35	0.38			99.24	
LLV8-9	SWE	small core		55.80			27.22		9.71		0.89			5.77	0.46			99.85	
LLV62-1	ME	lg fsp lath core		54.75			27.50		10.13		0.64	0.55	0.08	5.41	0.37			99.42	
LLV62-2	ME	lg fsp lath rim		56.77			25.94		8.41		0.85	0.60	0.31	6.19	0.65			99.73	
LLV62-3	ME	lg fsp lath core		56.50			26.45		9.04		0.77	0.49	0.19	6.01	0.54			99.98	
LLV62-4	ME	lg fsp lath rim		59.62			24.19		6.49		0.95	0.32	0.30	6.67	1.47			100.01	
Groundmass***																			
LLV86-8	ME	glass	0.37	61.76	0.16	1.05	16.13	1.50	3.08	0.04	3.15			5.04	3.85	0.03	0.28	96.45	20
LLV74-9	ME	glass	0.13	67.12	0.00	1.05	14.00	0.25	0.47	0.00	2.66			4.62	5.92	0.01	0.36	96.59	15
LLV41-13	ME	finely crystalline feldspar	0.03	63.61	0.03	0.11	19.82	0.00	1.72	0.01	0.93			6.95	4.90	0.00	0.02	98.12	10

Analytical information:

* Analyses done with a 15 kV accelerating voltage and 20 nA probe current, with a focused 1 micrometer beam. Count times for all elements are 20 seconds, and background is counted for 10 seconds. Analytical precision, based on analyses of standard reference materials of similar composition to the unknowns (VG-2 and internal amphibole reference material) , are as follows (all in wt.%): SiO_2±0.26, TiO_2±0.05, Al_2O_3±0.31, MgO±0.07, CaO±0.09, MnO±0.06, FeO±0.2, Na_2O±0.14, K_2O±0.03

** Analyses done with a 15 kV accelerating voltage and 20-nA probe current, with a defocusing 10 micrometer beam. Count times for all elements except Sr and Ba are 20 seconds, and background is counted for 10 seconds. Sr and Ba counted for 60 seconds, and background for 30 seconds. Analytical precision, based on analyses of standard reference materials of similar composition to the unknowns (anorthite, albite) , are as follows (all in wt.%):SiO_2±0.43, Al_2O_3±0.23, CaO±0.26, FeO±0.08, Na_2O±0.20, K_2O±0.01.

***Analyses done with a 15 kV accelerating voltage and 10 nA probe current, with a defocusing beam between 10 and 25 micrometers in diameter. Count times for most elements are 20 seconds. Longer count times are used for S (30 sec.), Cl (40 sec.) and F (60 sec.). Background count times are half of peak count times. Analytical precision, based on analyses of standard reference materials of similar composition to the unknowns (VG-568; VG-2, and KN-18) , are as follows (all in wt.%): P_2O_5±0.03, SiO_2±0.77, SO_2±0.01, TiO_2±0.05, Al_2O_3±0.31, MgO±0.07, CaO±0.09, MnO±0.06, FeO±0.08, Na_2O±0.14, K_2O±0.08, Cl±0.02.

to 1.37±0.08 Ma, and Southwest Edifice plateau ages ranging from 3.04±0.12 Ma to 4.15±0.21 Ma.

Spectra from the 12 Main Edifice samples tend to be of higher quality (Fig. 8). The fraction of released ^{39}Ar constituting the plateau age ranged from 56% to 89% of the total ^{39}Ar. The low temperature steps of some samples are completely concordant (e.g., sample 24, sample 34), and others (e.g., sample 42, sample 78) have anomalously young low-temperature steps. Some spectra (e.g., sample 63, sample 43) have low-temperature steps with negative apparent ages, probably due to incompletely removed $^{12}C_3$ or $H^{35}Cl$ isobarically interfering with ^{36}Ar. High-temperature steps from samples of the Main Edifice are similarly variable, ranging from nearly concordant (e.g., sample 24, sample 59) to strongly discordant (e.g., sample 37, sample 58), with apparent ages as high as 5 to 9 Ma. These strongly discordant high-temperature steps may be due to excess ^{40}Ar release from melt inclusions in microphenocrysts, or alternatively may be artifacts related to high-temperature blank contributions from the resistance furnace.

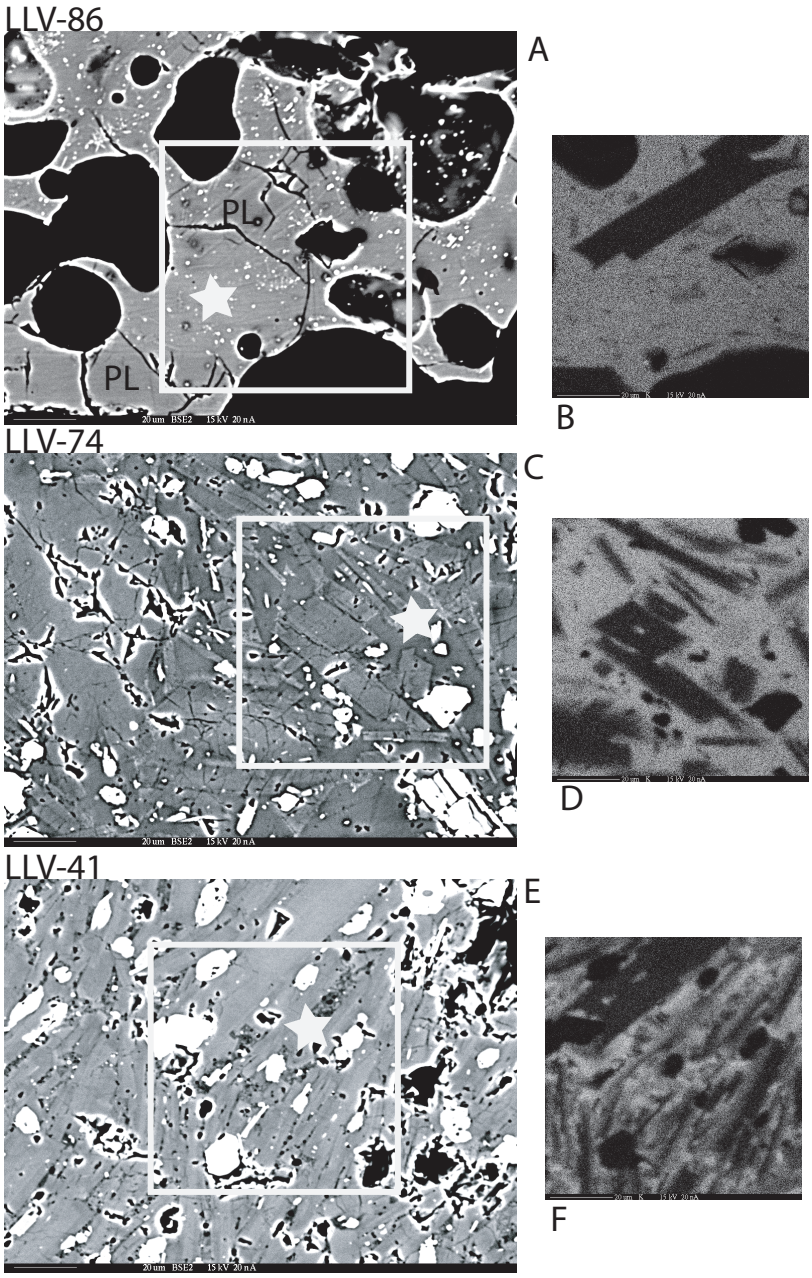


FIGURE 5. Backscattered electron (BSE) images (**A**, **C**, and **E**) and K-distribution maps (**B**, **D**, and **F**) for three samples from Los Lunas volcano, representing glassy, moderately crystalline, and holocrystalline end members. In the BSE images, areas that are brighter represent parts of the sample with higher mean atomic number (epoxy is black). The lath-like shapes in the BSE images are plagioclase microlites (labeled PL on image A), and the brightest areas are Fe-Ti oxide microlites. Areas between the plagioclase microlites are glassy in the cases of A and C, and microcrystalline in the case of E. K distribution maps correspond to areas outlined in white on the BSE images. White stars show locations of quantitative analyses presented in Table 2. Scale bars on all images are 20 μm in length. The sample shown in **A** and **B** was ranked 2, **C** and **D** ranked 5, and **E** and **F** ranked 9 (see description of ranking system in "Discussion" section).

K/Ca ratios, calculated from measured $^{40}Ar/^{39}Ar$ for the 12 samples from the Main Edifice are typical of basaltic to intermediate groundmass, with values near 1 for initial heating steps, steadily dropping to ~0.2 by the final temperature steps. Similar progressively dropping K/Ca values are typical for basaltic to intermediate groundmass analyzed by the $^{40}Ar/^{39}Ar$ method, and result from initial degassing of relatively K-rich, Ca-poor phases, chiefly plagioclase and glass, followed by higher-temperature degassing of relatively Ca-rich, K-poor phases, mainly pyroxene. Radiogenic yields (% of ^{40}Ar that is non-atmospheric) vary considerably among samples of the Main Edifice. Yields tend to be lowest for low- and high-temperature steps, and highest for intermediate-temperature steps. Maximum radiogenic yields for Main Edifice samples range from 6.3% (sample 43) to 70.1% (sample 42).

Age spectra from all seven samples from the Southwest Edifice are all somewhat more discordant than spectra from the Main Edifice samples. The fraction of released ^{39}Ar constituting the plateau ranges from 51% to 80% of the total ^{39}Ar released. The magnitude of discordance of low-and high-temperature steps tends to be greater than those of Main Edifice samples. Four samples have relatively concordant initial steps (samples 9, 12,17,68), whereas three (samples 14, 47,65) have strongly rising initial steps constituting >30% of released ^{39}Ar, possibly indicative of ^{40}Ar loss. Spectra from all seven samples have elevated high temperature steps with apparent ages ranging for 4.5 to 9 Ma. Southwest Edifice samples have falling K/Ca release patterns similar to Main Edifice samples, and maximum radiogenic yields that range from 11.8% (sample 65) to 55.9% (sample 68).

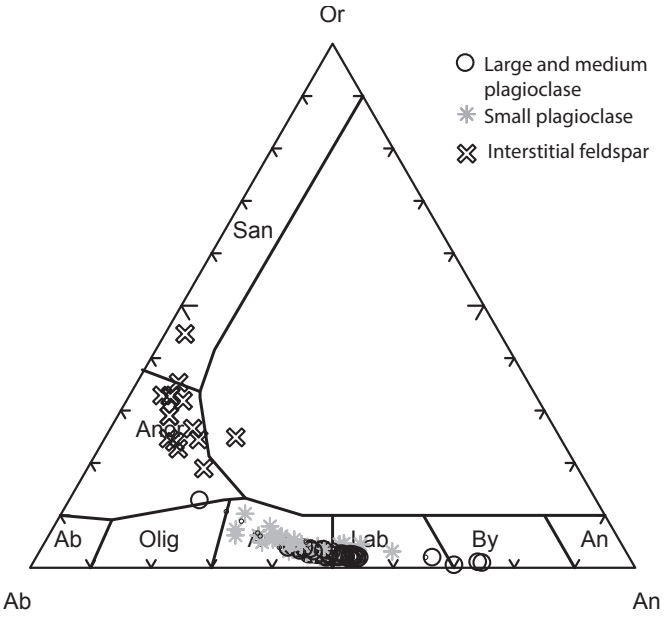


FIGURE 6. Feldspar composition from Los Lunas volcano, as analyzed by electron microprobe. Analytical uncertainly is similar to symbol size.

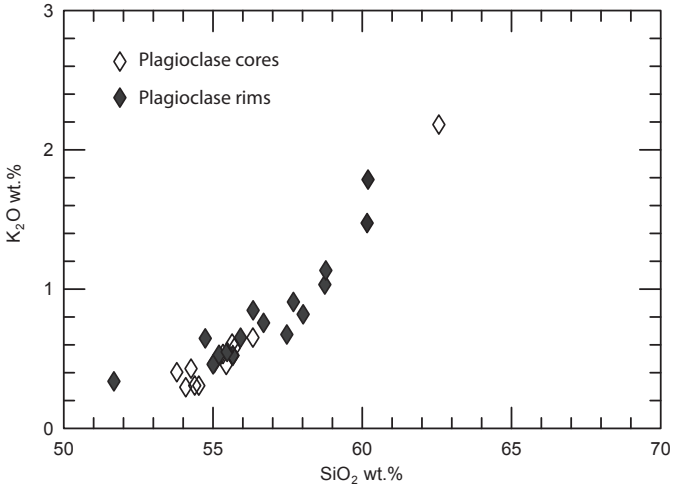


FIGURE 7. SiO_2 vs. K_2O (in wt.%) content of plagioclase cores and rims from Los Lunas volcano lava flows, as analyzed by electron microprobe. Analytical uncertainty is similar to symbol size.

DISCUSSION

Microprobe Sample Evaluation and Quality of $^{40}Ar/^{39}Ar$ Results

In this study, microprobe assessment proved to be effective for predicting the quality of $^{40}Ar/^{39}Ar$ age data. For age spectra from both Main Edifice and Southwest Edifice samples, our microprobe assessment rating appears to correlate well with $^{40}Ar/^{39}Ar$ data quality (Table 3, Figs. 8, 9, 10 and 11). After using the microprobe to rate potential samples on a scale of 1 to 10, a total of 19 samples were selected from samples with ratings of 6 to 10. All of the selected samples yielded spectra sufficiently flat to meet plateau criteria; it is likely that highly discordant results were avoided by rejecting samples with ratings of 5 or less. Within the group of highly rated samples, higher quality results were obtained from nearly all samples rated 8 or higher, and samples rated 6 or 7 yielded lower quality results. The relationships between microprobe ratings and various indicators of age data quality are summarized in Figure 11. Indications of higher quality results include generally higher maximum radiogenic yields (Fig. 11C-D), less discordance at high-and low-temperature ends of the age spectra, as shown by higher percent ^{39}Ar released in the plateau segment (Fig. 11A-B), and less precise ages for individual steps and for age plateaus (Fig. 10, Table 3).

Based on the combination of relatively low microprobe rating (6 or 7) and low data quality, we suggest that results from eight of the 19 samples are likely to be inaccurate, and we have excluded these data from mean-age calculations (Table 3, Fig. 10). Samples included in mean age calculations have probe ratings of 8 to 10, and highly precise plateau ages with two sigma uncertainties less than ± 2% (Table 3). Excluded samples were selected on the basis of probe ratings of 6 to 7, low yields, and low temperature discordance. These include samples 43, 63, 78, and 73 from the Main Edifice, and samples 14, 467, and 65 from the Southwest Edifice. Two exceptions include sample 37 from the Main Edifice, which was included because of high data quality in spite of a microprobe rating of 7, and sample 17 from the Southwest Edifice (Fig. 11), which, in spite of a probe rating of 10, has a low precision plateau age.

We interpret the lower quality age data from samples with lower microprobe ratings as a direct consequence of even small amounts of groundmass glass, which results in atmospheric argon being acquired during hydration, ^{40}Ar or K_2O loss, and ^{39}Ar recoil artifacts, and the higher quality age data from samples with higher microprobe ratings as a consequence of most K being in a feldspar, which is less subject to the problems mentioned above, rather than in glass. However, although the microprobe ratings are a strong predictor of data quality, in a few cases there is a disconnect between age quality and microprobe rating, possibly due to sample heterogeneity either in terms of alteration or crystallization.

Chronology of Los Lunas Volcano

The results from the highest-ranking samples indicate that the Los Lunas volcano was erupted during two brief phases of activity, which is consistent with field observations. The Southwest Edifice was erupted chiefly at 3.83±0.05 Ma (mean age of three samples). After a 2.6-Ma-long eruptive hiatus, the Main Edifice was erupted at 1.271±0.014 Ma (mean age of 8 samples). Field observations indicate that emplacement of the Main Edifice included at least five distinct lava flows, but the high precision $^{40}Ar/^{39}Ar$ ages suggest that all of these events took place within a time span of less than 100,000 years. The age determined for the Main Edifice is slightly older than the 1.24-Ma upper Bandelier (Tshirege) ash fall deposit, which overlies the Main Edifice in a sedimentary sequence exposed in a canyon on the north side of the volcano.

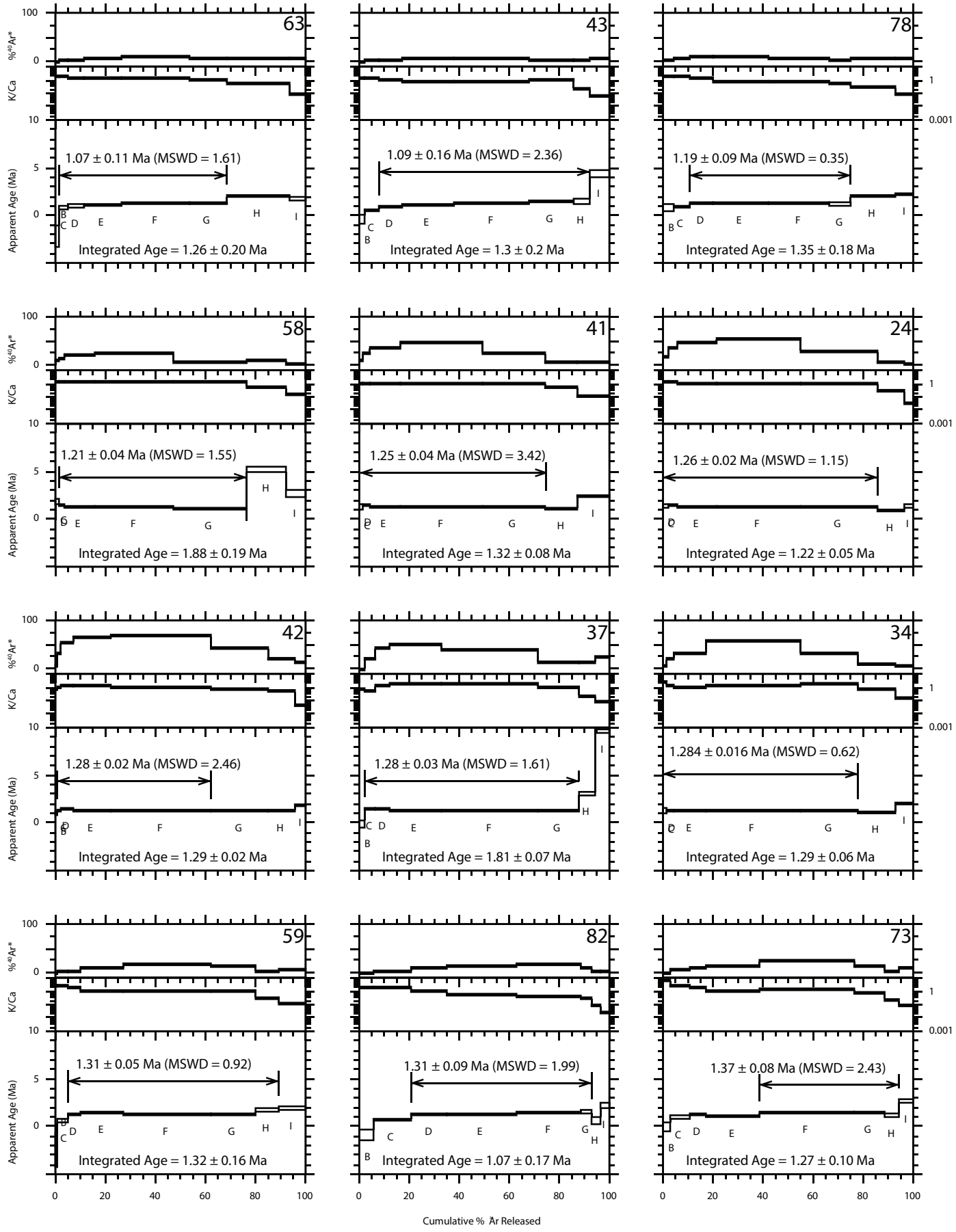

63
1.07 ± 0.11 Ma (MSWD = 1.61)
Integrated Age = 1.26 ± 0.20 Ma
43
1.09 ± 0.16 Ma (MSWD = 2.36)
Integrated Age = 1.3 ± 0.2 Ma
78
1.19 ± 0.09 Ma (MSWD = 0.35)
Integrated Age = 1.35 ± 0.18 Ma
58
1.21 ± 0.04 Ma (MSWD = 1.55)
Integrated Age = 1.88 ± 0.19 Ma
41
1.25 ± 0.04 Ma (MSWD = 3.42)
Integrated Age = 1.32 ± 0.08 Ma
24
1.26 ± 0.02 Ma (MSWD = 1.15)
Integrated Age = 1.22 ± 0.05 Ma
42
1.28 ± 0.02 Ma (MSWD = 2.46)
Integrated Age = 1.29 ± 0.02 Ma
37
1.28 ± 0.03 Ma (MSWD = 1.61)
Integrated Age = 1.81 ± 0.07 Ma
34
1.284 ± 0.016 Ma (MSWD = 0.62)
Integrated Age = 1.29 ± 0.06 Ma
59
1.31 ± 0.05 Ma (MSWD = 0.92)
Integrated Age = 1.32 ± 0.16 Ma
82
1.31 ± 0.09 Ma (MSWD = 1.99)
Integrated Age = 1.07 ± 0.17 Ma
73
1.37 ± 0.08 Ma (MSWD = 2.43)
Integrated Age = 1.27 ± 0.10 Ma
%40Ar*
K/Ca
Apparent Age (Ma)
Cumulative % 39Ar Released

Table 3. Summary of 40Ar/39Ar results from groundmass concentrates from Los Lunas Volcano samples.

Plateau Age													
Sample	**Rock type**	**Probe rating**	**L#**	**n**	**%^{39}Ar**	**MSWD**	**K/Ca**	**±**	**2s**	**max ^{40}Ar***	**Age(Ma)**	**±**	**2s**
Main Edifice samples													
98LL-63	lava	6	52270-01	5	67.4	1.6	1.3	±	0.8	8.8	1.07	±	0.11
98LL-43	lava	6	52282-01	5	84.3	2.4	0.8	±	0.6	6.3	1.09	±	0.16
98LL-78	lava	7	52268-01	4	64.1	0.4	0.8	±	0.7	10.0	1.19	±	0.09
98LL-58	lava	8	52269-01	4	75.5	1.6	1.3	±	0.3	24.8	1.21	±	0.04
98LL-41	lava	9	52277-01	5	74.4	3.4	1.0	±	0.1	46.1	1.25	±	0.04
98LL-24	lava	9	52283-01	6	85.8	1.2	1.0	±	0.4	54.6	1.26	±	0.02
98LL-42	lava	9	52266-01	5	84.5	4.7	1.1	±	0.4	70.1	1.28	±	0.03
98LL-37	lava	7	52272-01	5	85.8	1.6	1.5	±	0.8	50.6	1.28	±	0.03
98LL-34	lava	9	52267-01	6	78.0	0.6	1.5	±	1.4	56.2	1.28	±	0.02
98LL-59	lava	9	52279-01	5	84.5	0.9	1.0	±	1.0	18.7	1.31	±	0.05
98LL-82	lava	8	52271-01	4	72.4	2.0	0.6	±	0.6	19.2	1.31	±	0.09
98LL-73	lava	6	52273-01	3	55.9	2.4	1.0	±	1.0	26.4	1.37	±	0.08
Main Edifice mean age				**8**			**2.33**				**1.271**	**±**	**0.014**
Southwest Edifice samples													
98LL-47	lava	6	52278-01	3	51.2	2.8	0.6	±	0.3	38.2	3.04	±	0.12
98LL-14	lava	6	52265-01	4	60.8	0.2	0.5	±	0.3	21.1	3.15	±	0.13
98LL-65	lava	7	52275-01	3	50.9	0.1	0.5	±	0.1	11.8	3.29	±	0.28
98LL-68	lava	10	52276-01	3	73.0	2.1	1.1	±	0.6	55.9	3.80	±	0.06
98LL-09	intrusive	10	52280-01	7	79.6	2.1	0.9	±	0.4	34.6	3.86	±	0.10
98LL-12	intrusive	9	52281-01	6	72.3	1.8	1.2	±	0.9	35.5	3.88	±	0.08
98LL-17	lava	10	52274-01	3	77.3	1.8	1.11.8	±	0.5	29.9	4.15	±	0.21
Southwest Edifice mean age				**3**			**1.44**				**3.83**	**±**	**0.05**

Note: Ages in bold are used in mean-age calculations; ages not in bold were rejected because of poor data quality and/or microprobe assessment rating of 7 or less all ages relative to Fish Canyon Tuff Sanidine At 28.201 Ma (Kuiper et al., 2008); unit is map unit assigned by Panter et al.(1999);

L# is laboratory number; n is number of steps on age plateau, %^{39}Ar is percent of ^{39}Ar released in age plateau; MSWD is mean square of weighted deviates; K/Ca is elemental ratio determined from measured ^{37}Ar/^{39}Ar; max %^{40}Ar* is highest radiogenic yield achieved during incremental heating.

Sample information in Supplementary Documentation Table 1

Whole Rock Geochemistry

The broadly similar composition and overlapping construction of the two edifices that constitute the Los Lunas volcanic complex suggest that their petrogenetic relationship should be examined. One possibility is that the dacitic magma of the older Southwest Edifice may have been derived from a parental melt with composition similar to the trachyandesite of the younger Main Edifice by simple closed-system fractional crystallization of pyroxenes, feldspars, apatite and spinel, which might explain trends of decreasing MgO, TiO_2, FeO_t, CaO, P_2O_5, Sr, and Ba with increasing SiO_2 concentration (Figs. 3-4). However, several observations suggest that a simple, single liquid-line-of-descent between the two compositional types is unlikely.

For example, the en echelon trends in the data that are displayed on the MgO versus SiO_2 plot in Figure 3E would be difficult to explain by a simple model of progressive fractionation of MgO-rich phases from a single parent. It is also difficult to unravel the cause for variations in K_2O, Sr, Rb and Ba with SiO_2 as shown in Figures 3F and 4A, B and D. These elements are compatible in one or more of the minerals amphibole, biotite and feldspar that have measured partition coefficients that are mostly greater than 2.0 (some >10) for dacites and rhyolites (Ewart and Griffin, 1994; Philpotts and Schnetzler, 1970). While the fractionation of plagioclase and biotite could explain the overall decrease in Sr and Ba with increasing silica (Figs. 4A- B), the increase in K_2O and Rb for trachyandesite (Figs. 3F and 4D) would suggest the opposite. The ill-defined negative trends for dacite on the same plots, however, may signify

FIGURE 8. ^{40}Ar/^{39}Ar incremental heating spectra from samples of the Main Edifice of Los Lunas volcano. Samples are in the same order as in Table 3. Individual spectra titles identify results that were rejected because of low microprobe rating or poor data quality. Uncertainties on individual steps and on plateau ages are two sigma. Sample names are shown in upper right corner of the spectra.

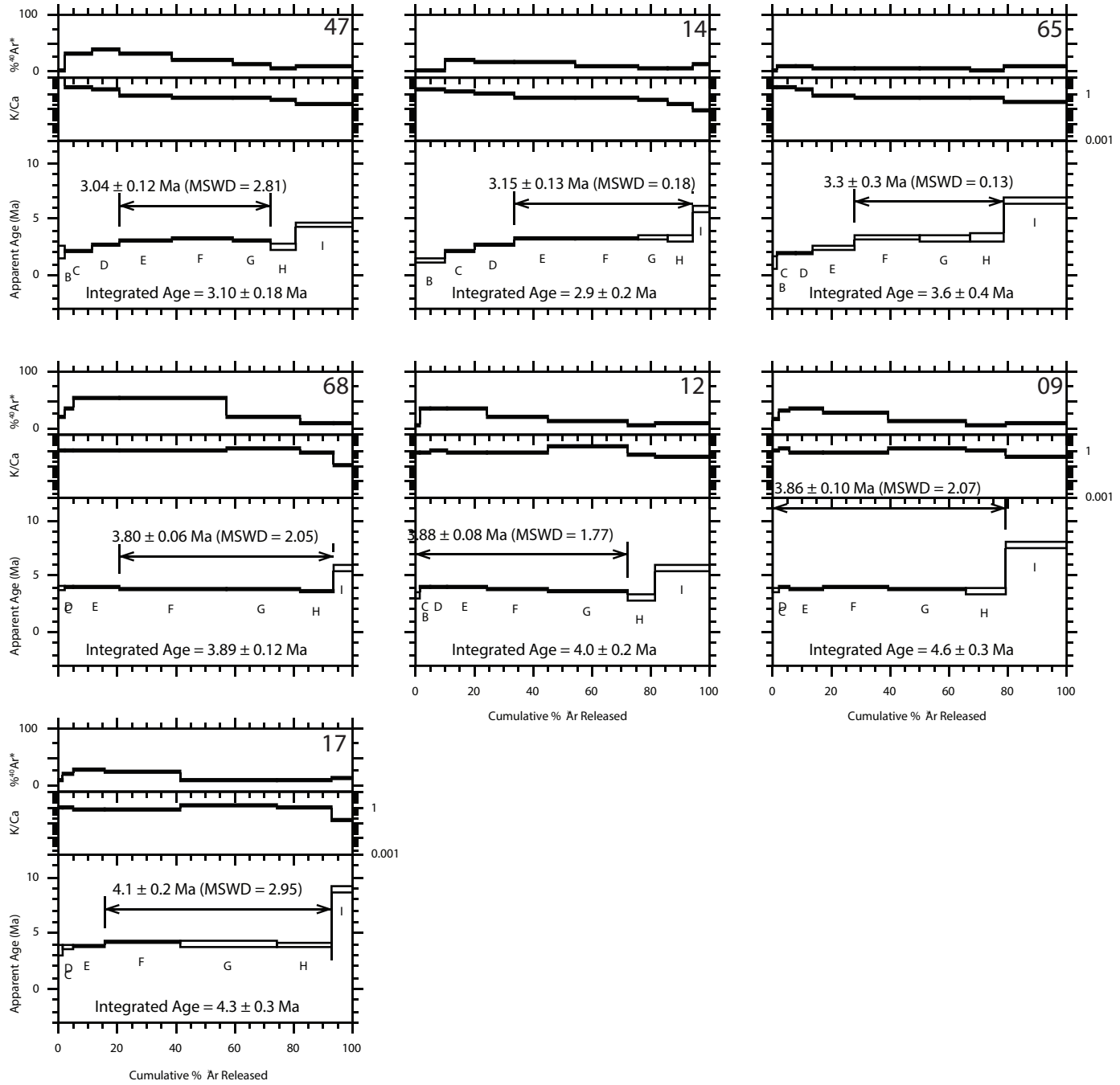


FIGURE 9. $^{40}Ar/^{39}Ar$ incremental heating spectra from samples of the Southwest Edifice of Los Lunas volcano. Samples are in the same order as in Table 3. Individual spectra titles identify results that were rejected because of low microprobe rating or poor data quality. Uncertainties on individual steps and on plateau ages are two sigma. Sample names are shown in upper right corner of the spectra.

the removal of amphibole (K $K_d^{amp\text{-}melt} > 24$; (Nagasawa and Schnetzler, 1971)) and biotite (Rb $K_d^{bt\text{-}melt} > 5$; Ewart and Griffin, 1994) from magmas that would define the high K_2O and Rb end of the trachyandesite array.

Further testing using quantitative models for fractional crystallization is needed but is beyond the scope of this paper. The assessment of open-system processes (i.e., assimilation-fractional crystallization and magma mixing) is also necessary with the aid of a full suite of trace elements and radiogenic isotopes (e.g., Sr, Nd, Pb) in order to fully decipher magma origin and evolution at the Los Lunas volcano. The simplest explanation, given the geochemical data and age difference between the two edifices, is that although the two eruptive events may have both been structurally controlled by the same zone of crustal weakness, the magma batches that formed the two edifices are not genetically related.

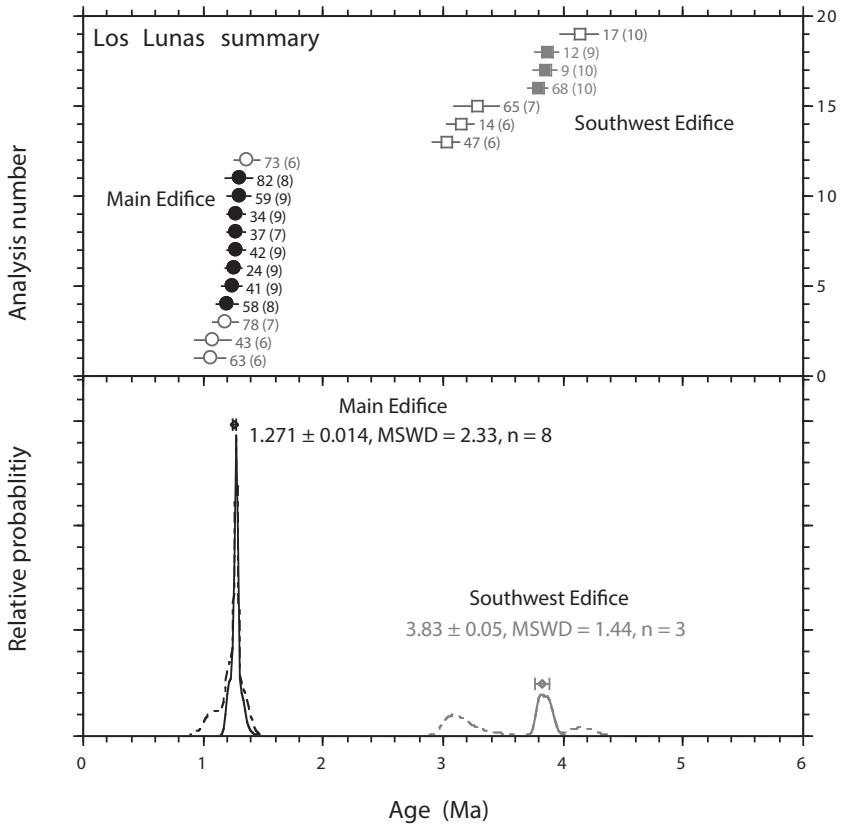


FIGURE 10. Probability distribution diagram showing $^{40}Ar/^{39}Ar$ plateau ages from all dated samples. Upper panel shows plateau ages with one sigma errors. Individual plateau ages are identified by sample number followed by microprobe rating in parentheses. Hollow symbols denote results that that were rejected because of low microprobe rating or poor data quality. The lower panel provides probability distribution diagrams and weighted mean ages for the Main and Southwest Edifices. Weighted mean age errors are two sigma.

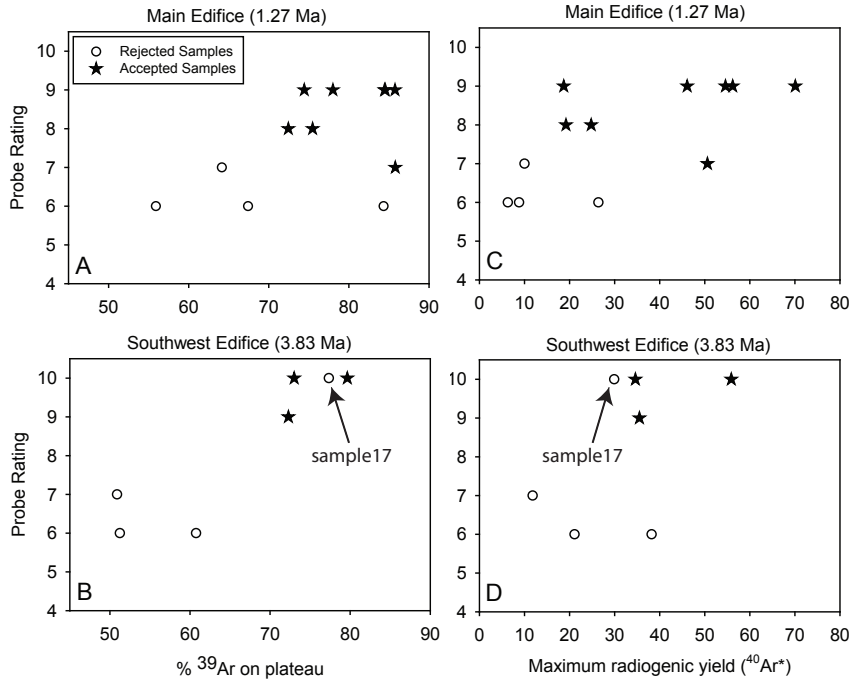


FIGURE 11. Comparisons of microprobe ratings versus data quality parameters for samples from the Main Edifice (A, C) and the Southwest Edifice (B, D).

CONCLUSIONS

1. To obtain the best possible $^{40}Ar/^{39}Ar$ ages on extrusive mafic rocks, selecting the least-glassy rock in the field, and examining the rock in thin section is a good start. However, the quality of dates produced by $^{40}Ar/^{39}Ar$ analysis of young, low -K, extrusive rocks can be much improved by using the electron microprobe to rank the quality of potential dating samples. The criteria for selection of the best possible samples includes complete or near complete crystallization of interstitial residual glass, the absence of alteration phases, and the presence of potassium-bearing feldspar, either as a fine-grained groundmass phase, or as rims on larger plagioclase.

2. Higher ranked samples tend to have relatively flat age spectra, higher radiogenic yields, and more precise plateau ages represented by larger fractions of ^{39}Ar released. Lower ranked samples are also more likely to be anomalously young or anomalously old relative to the mean age of higher ranked samples.

3. Microprobe assessment of lava samples prior to carrying out geochronology saves time, and therefore money. The microprobe assessment can be done in roughly two hours, and over half of this time is devoted to automated analysis (elemental maps and quantitative analysis). Also, with a small amount of addition effort, the mineral chemistry of the sample can be assessed, which can be useful information for petrological investigation of the volcanic system. Once this assessment is done, only the best-suited samples can move forward for time-consuming sample preparation and age determinations.

4. The Los Lunas volcano underwent two distinct phases of eruptive activity, consistent with field mapping. The first, here called the Southwest Edifice, occurred at around 3.83 Ma. The second event, which formed the Main Edifice, took place at 1.27 Ma, and consisted of at least five eruptive episodes that spanned of less than 100,000 years.

5. Geochemical evidence does not support a genetic relationship between the older and younger magma batches, suggesting that the spatial relationship between the two volcanic edifices may be solely a function of the presence of a zone of crustal weakness that allowed the magmas to rise and erupt at similar locations.

REFERENCES

Bachman, G. O., and Mehnert, H. H., 1978, New K-Ar dates and the late Pliocene to Holocene geomorphic history of the central Rio Grande region, New Mexico: Geological Society of America Bulletin, v. 89, p. 283-292.

Dalrymple, G. B., 1969, $^{40}Ar/^{36}Ar$ analyses of historic lava flows: Earth and Planetary Science Letters, v. 6, p. 47-55.

Dalrymple, G. B., and Moore, J. G., 1968, Argon-40 excess in submarine pillow basalts from Kilauea volcano, Hawaii: Science, v. 161, p. 1132-1135.

Esser, R., McIntosh, W., Heizler, M., and Kyle, P., 1997, Excess argon in melt inclusions in zero-age anorthoclase feldspar from Mt. Erebus, Antarctica, as revealed by the $^{40}Ar/^{39}Ar$ method: Geochimica et Cosmochimica Acta, v. 61, p. 3789-3801.

Ewart, A., and Griffin, W. L., 1994, Application of proton-microprobe data to trace-element partitioning in volcanic rocks: Chemical Geology, v. 117, p. 251-284.

Fleck, R. J., Sutter, J. F., and Elliot, D. H., 1977, Interpretation of discordant 40Ar/39Ar age spectra of Mesozoic tholeiites from Antarctica: Geochimica Cosmochimica Acta, v. 41, p. 15-32.

Foland, K. A., Fleming, T. H., Heimann, A., and Elliot, D. H., 1993, Potassium-argon dating of fine-grained basalts with massive Ar loss: Application of the 40Ar/39Ar technique to plagioclase and glass from the Kirkpatrick Basalt, Antarctica: Chemical Geology, v. 107, p. 173-190.

Irvine, T. N., and Braragar, W. R., 1971, A guide to the chemical classification of the common igneous rocks: Canadian Journal of Earth Sciences, v. 8, p. 523-548.

Kasten, J. A., 1977, Petrology and geochemistry of calc-alkaline andesites within the Albuquerque Basin, Valencia County, New Mexico [M.S. thesis]: Albuquerque, University of New Mexico, 79 p.

Kelley, V. C., and Kudo, A. M., 1978, Volcanoes and related basalts of Albuquerque Basin, New Mexico: New Mexico Bureau of Mines and Mineral Resources, Circular 156, 30 p.

Koppers, A. A. P., Staudigel, H., and Wijbrans, J. R., 2000, Dating crystalline groundmass separates of altered Cretaceous seamount basalts by the $^{40}Ar/^{39}Ar$ incremental heating technique: Chemical Geology, v. 166, p. 139-158.

Kuiper, K. F., Deino, A., Hilgen, F. J., Krijgsman, W., Renne, P. R., and Wijbrans, J. R., 2008, Synchronizing rock clocks of Earth history: Science, v. 320, p. 500-504.

Love, D. W., Maldonado, F., Hallett, B., Panter, K., Reynolds, C., McIntosh, W. C., and Dunbar, N. W., 1998, Preliminary geologic map of the Dalies Quadrangle, Valencia County, New Mexico. New Mexico Bureau of Geology and Mineral Resources, Open-file Map 21, scale 1:24,000.

Nagasawa, H., and Schnetzler, C. C., 1971, Partitioning of rare Earth, alkali, and alkaline Earth elements between phenocrysts and acidic igneous magmas. : Geochimica et Cosmochimica Acta, v. 35, p. 953-968.

Nielsen, C. H., and Sigurdsson, H., 1981, Qualitative methods for electron microprobe analysis of sodium in natural and synthetic glasses: American Mineralogist, v. 66, p. 547-552.

Panter, K., Hallett, B., Love, D., McKee, C., and Thompson, R., 1999, A volcano revisited: A preliminary report of the geology of Los Lunas Volcano, Central New Mexico: New Mexico Geology, v. 21, p. 44.

Philpotts, J. A., and Schnetzler, C. C., 1970, Potassium, rubidium, strontium, barium, and rare-Earth concentrations in lunar rocks and separated phases: Science, v. 167, , p. 493-495.

Rowe, M. C., Wolff, J. A., Gardner, J. N., Ramos, F. C., Teasdale, R., and Heikoop, C. E., 2007, Development of a continental volcanic field: Petrogenesis of pre-caldera intermediate and silicic rocks and origin of the Bandelier magmas, Jemez Mountains (New Mexico, USA): Journal of Petrology, v. 48, p. 2063-2091.

Singer, B. S., and Pringle, M. S., 1996, Age and duration of the Matuyama-Brunhes geomagnetic polarity reversal from $^{40}Ar/^{39}Ar$ incremental heating analyses of lavas: Earth and Planetary Science Letters, v. 139, p. 47-61.

Singer, B. S., Wijbrans, J. R., Nelson, S. T., Pringle, M. S., Feeley, T. C., and Dungan, M. A., 1998, Inherited argon in a Pleistocene andesite lava; (super 40) Ar/ (super 39) Ar incremental-heating and laser-fusion analyses of plagioclase: Geology, v. 26, p. 427-430.

Winick, J. A., McIntosh, W. C., and Dunbar, N. W., 2001, Melt-inclusion-hosted excess ^{40}Ar in quartz crystals of the Bishop and Bandelier magma systems: Geology, v. 29, p. 275-278.

Supplemental data can be found at http://nmgs.nmt.edu/repository/index.cfml?rid=2016001